Exciton dynamics in emergent Rydberg lattices

S. Bettelli,[1] D. Maxwell,[2] T. Fernholz,[1] C. S. Adams,[2] I. Lesanovsky,[1] and C. Ates[1]

[1]*School of Physics and Astronomy, The University of Nottingham, University Park, NG7 2RD Nottingham, United Kingdom*

[2]*Joint Quantum Centre (JQC) Durham-Newcastle, Department of Physics, Durham University, Durham DH1 3LE, United Kingdom*

(Received 7 June 2013; revised manuscript received 16 September 2013; published 31 October 2013)

The dynamics of excitons in a one-dimensional ensemble with partial spatial order are studied. During optical excitation, cold Rydberg atoms spontaneously organize into regular spatial arrangements due to their mutual interactions. This emergent lattice is used as the starting point to study resonant energy transfer triggered by driving a nS to $n'P$ transition using a microwave field. The dynamics are probed by detecting the survival probability of atoms in the nS Rydberg state. Experimental data qualitatively agree with our theoretical predictions including the mapping onto the XXZ spin model in the strong-driving limit. Our results suggest that emergent Rydberg lattices provide an ideal platform to study coherent energy transfer in structured media without the need for externally imposed potentials.

DOI: 10.1103/PhysRevA.88.043436 PACS number(s): 32.80.Ee, 32.80.Qk, 67.85.−d, 71.35.Aa

I. INTRODUCTION

The investigation of far-from-equilibrium phenomena overarches the fields of physics, chemistry, and biology. Systems out of equilibrium feature fascinating phenomena such as the formation of complex-ordered structures in spite of a rather simple underlying microscopic description [1]. Moreover, dynamical phenomena such as resonant energy transfer are of central practical importance as they underlie many fundamental physical processes in molecular aggregates [2], photosynthesis [3], and novel materials such as organic solar cells [4].

Gases of cold atoms have been established in the past years as a platform which permits the detailed investigation of systems in and out of equilibrium [5–7]. Recently atoms excited to high-lying Rydberg states have become a major focus due to their strong interactions over large distances (several micrometers) and short time scales (nanoseconds) allowing to address fundamental questions in many-body physics. On the one hand, the strong interactions give rise to the phenomenon of dipole blockade [8], which prevents simultaneous photoexcitation of nearby atoms. On the other hand, the large dipole moments associated with electronic transitions among Rydberg states lead to fast resonant energy transfer over long distances.

Dipole blockade has been widely exploited for applications in quantum information processing [9] and quantum optics [10–15]. In the many-body context, spatial correlations of laser-excited atoms were recently investigated theoretically in one-dimensional finite-size samples [16–19]. It was found that at high atomic density the distribution of the Rydberg atoms can become highly structured leading in the extreme case to the spontaneous formation of small ordered patches consisting of a few Rydberg atoms. From the experimental side much effort has been invested to probe these spatial correlations [20–22]. In parallel, resonant energy transfer has been the focus of pioneering experiments on cold (frozen) Rydberg gases [23,24]. Spectral broadening of Rydberg lines could be attributed to coherent electronic energy transfer between Rydberg atoms. These findings have ushered further experimental [25–28] as well as theoretical [29–37] efforts to analyze excitonic transfer processes and their consequences in cold Rydberg systems.

In this work we build on these developments and present a study of the out-of-equilibrium behavior of Rydberg gases that directly links to the above-mentioned themes of order formation and excitation transfer. We explore the electronic dynamics of a (quasi) one-dimensional Rydberg gas within a two-step protocol, see Fig. 1. In step 1, high-lying Rydberg nS states are optically excited leading to the spontaneous emergence of a lattice of Rydberg atoms immersed in the atomic gas of ground-state atoms. In the subsequent step 2 we trigger coherent excitation transfer between Rydberg atoms by the excitation of nearby Rydberg $n'P$ states via a microwave field. We theoretically investigate the resulting nonequilibrium exciton dynamics through the analysis of the survival probability of atoms in the Rydberg nS state. We show that the survival probability has a characteristic dependence on the spatial arrangement as well as on the number of Rydberg atoms and derive an effective Hamiltonian in the limit of strong microwave driving. We compare our theoretical predictions with an experiment in which the survival probability is measured through an optical readout protocol and find qualitative agreement. Our work shows the versatility of homogeneous gases of Rydberg atoms for the study of nonequilibrium processes such as coherent transport phenomena.

The paper is organized as follows. In Sec. II we theoretically describe and investigate the spontaneous formation of lattices of Rydberg atoms upon photoexcitation from a one-dimensional finite-size atomic gas. Subsequently, we discuss the electronic dynamics when the excited atoms are coupled to a nearby Rydberg state by a microwave (Sec. III). In particular, we illuminate on the connection between the electronic dynamics with the underlying ordering of the Rydberg atoms. Finally, in Sec. IV we present experimental data that are obtained using a similar protocol as the one discussed in this work and find qualitative agreement between the experiment and theory. Unless stated otherwise we will work in units where $\hbar = 1$.

II. EMERGENT LATTICE

First we introduce the framework within which we describe exciton dynamics in an emergent lattice (cf. Fig. 1). We consider a one-dimensional atomic gas of length L with

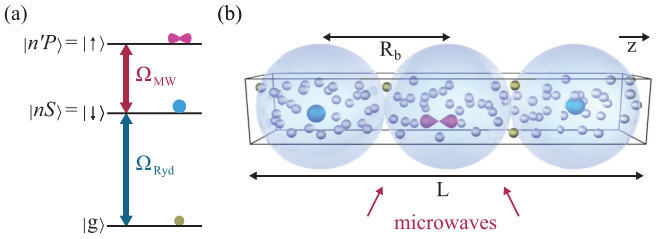

FIG. 1. (Color online) (a) Rydberg levels and excitation scheme. In step 1 atoms are optically excited from their electronic ground state $|g\rangle$ to a highly excited state $|nS\rangle$ with effective Rabi frequency $\Omega_{\rm Ryd}$. Subsequently, in step 2, a microwave field is applied that couples the $|nS\rangle$ state to a nearby $|n'P\rangle$ level with Rabi frequency $\Omega_{\rm MW}$. These states are identified as internal states of a fictitious spin-1/2 particle. (b) Quasi-one-dimensional geometry of the system. The large van der Waals potential between the $|nS\rangle$ Rydberg atoms (blue spheres) induces an exclusion volume around each excited atom characterized by the blockade radius R_b larger than the transverse size of the sample. This leads to a highly structured density distribution of the Rydberg atoms after the laser excitation step. The transition dipole-dipole interaction induces a coherent spatial transfer of $(n'P)$ excitations.

homogeneous density $\rho = N/L$, where N denotes the total number of atoms and we set our quantization axis (z) along the long axis of the gas. To describe the electronic dynamics, we use a simplified level scheme in which each atom is modeled by using three levels: the electronic ground state $|g\rangle$ and two dipole-coupled, highly excited states $|nS\rangle$ and $|n'P\rangle$ with principal quantum numbers n and n' and angular momentum $l = 0$ (S) and $l = 1$ (P), respectively. The actual states used in the experiment will be discussed later.

In the first step of our protocol, atoms are optically excited from $|g\rangle$ to $|nS\rangle$. The dynamics in this step are dominated by the strong van der Waals interaction between Rydberg atoms. Such interactions shift many-body states containing pairs of Rydberg atoms closer than a critical distance out of resonance. Consequently each excited atom is surrounded by a blockade volume of radius R_b, within which no further Rydberg excitations are found. For our finite, one-dimensional, homogeneous system this dipole blockade mechanism restricts the maximum number of Rydberg excitations to $\nu_{\max} = \lfloor L/R_b \rfloor + 1$, where $\lfloor x \rfloor$ denotes the closest integer smaller than x. We have assumed a sharply defined blockade volume which is justified in the case of a one-dimensional system and rapidly decaying van der Waals interaction [16,38]. The quantum state after the laser excitation (i.e., the initial state of the microwave driving) can be formally written as

$$|\Psi_0\rangle = \sum_{\nu=0}^{\nu_{\max}} \sum_{1\leqslant\alpha_1<\cdots<\alpha_\nu\leqslant N} g^{(\nu)}_{\alpha_1,\ldots,\alpha_\nu} \left(\prod_{j=1}^{\nu} e^{-ikz_{\alpha_j}} S^+_{\alpha_j}\right) |0\rangle. \quad (1)$$

Here, $|0\rangle = \bigotimes_i |g\rangle_i$ is the Rydberg vacuum, $S^+_i = |nS\rangle\langle g|_i$ is the operator that creates a Rydberg atom at position z_i and k is the total momentum imposed by the excitation laser(s), where we assume $\hat{k} \parallel \hat{z}$. In general, this state is highly correlated and the coefficients $g^{(\nu)}_{\alpha_1,\ldots,\alpha_\nu} \equiv g^{(\nu)}(z_{\alpha_1},\ldots,z_{\alpha_\nu})$ depend on the positions of all excited atoms and on time (the time label was suppressed to shorten the notation). These correlations, which dynamically build up during the laser excitation, render a full quantum calculation of $|\Psi_0\rangle$ a formidable task.

However, as was recently shown numerically [39] and analytically [40,41], for sufficiently large times the strong interactions between Rydberg atoms result in an equilibration. In this saturated regime the moduli of the coefficients $g^{(\nu)}$ of configurations compatible with the Rydberg blockade *become equal and constant in time* [16]. Therefore, observables that depend only on the $|g^{(\nu)}|^2$, such as the Rydberg density and density-density correlations, attain a stationary value. To calculate such "classical observables" we use a Monte Carlo method that allows us to sample arrangements of Rydberg atoms compatible with the excitation blockade. The details of the algorithm are given in the Appendix A.

Figure 2(a) shows the numerically calculated stationary Rydberg density distributions as a function of the system length L for a gas consisting of $N = 10^4$ atoms at fixed blockade radius and open boundary conditions. For $L > R_b$ the plot shows a highly structured density distribution with pronounced peaks at the boundaries of the gas. Whenever the system size slightly exceeds an integer multiple of the blockade radius the density distribution closely resembles a lattice of Rydberg atoms, i.e., the excited atoms are arranged in the densest packing allowed by the excitation blockade. Similar structures have also been reported in [18,19,38]. We emphasize, however, that the emergence of such seemingly ordered structures is a finite-size effect, as for one-dimensional systems with finite-range interactions spatial correlations decay exponentially with increasing distance in the thermodynamic limit [16].

III. EXCITONIC DYNAMICS

Once the Rydberg lattice is created we trigger the excitonic dynamics by irradiating the ensemble with a microwave field (linearly polarized along the z axis and with Rabi frequency $\Omega_{\rm MW}$) that is resonant with the $|nS\rangle$-$|n'P\rangle$ transition as shown in Fig. 1(a). The corresponding transition dipole moment μ can reach thousands of atomic units (scaling as n^2 for $n = n'$). This results in a strong microwave coupling, but also induces a significant resonant dipole-dipole interaction enabling excitations to be exchanged coherently between atoms, i.e., two distant Rydberg atoms swap their electronic state according to $|nS\rangle_i|n'P\rangle_j \leftrightarrow |n'P\rangle_i|nS\rangle_j$. For the particular geometry of our system this resonant dipole-dipole interaction does not couple different magnetic sublevels and the electronic structure of each Rydberg atom reduces to that of an effective spin-1/2 particle where we identify $|nS\rangle \equiv |\downarrow\rangle$ and $|n'P\rangle \equiv |\uparrow\rangle$. In atomic units the interaction strength is given by $V_{ij} = (-2/3)\mu^2/|z_i - z_j|^3$, where z_i denotes the position of the ith Rydberg atom [30]. The Hamiltonian describing the resulting dynamics is given by

$$H = \frac{\Omega_{\rm MW}}{2} \sum_i \sigma^x_i + \sum_{ij,(i\neq j)} V_{ij}(\sigma^+_i\sigma^-_j + \sigma^-_i\sigma^+_j) \quad (2)$$

with $\sigma^\pm = (\sigma^x \pm i\sigma^y)/2$ and $\sigma^{x,y,z}$ denoting the usual Pauli spin matrices.

To study the excitonic dynamics we analyze the survival probability, $p_T(\Omega_{\rm MW}) \equiv |\langle\Psi_0|e^{-iHT}|\Psi_0\rangle|^2$, of the state $|\Psi_0\rangle$. The motivation behind choosing this quantity stems from the fact that $p_T(\Omega_{\rm MW})$ is accessible experimentally, as has been shown recently [28], and that its rich dynamical behavior

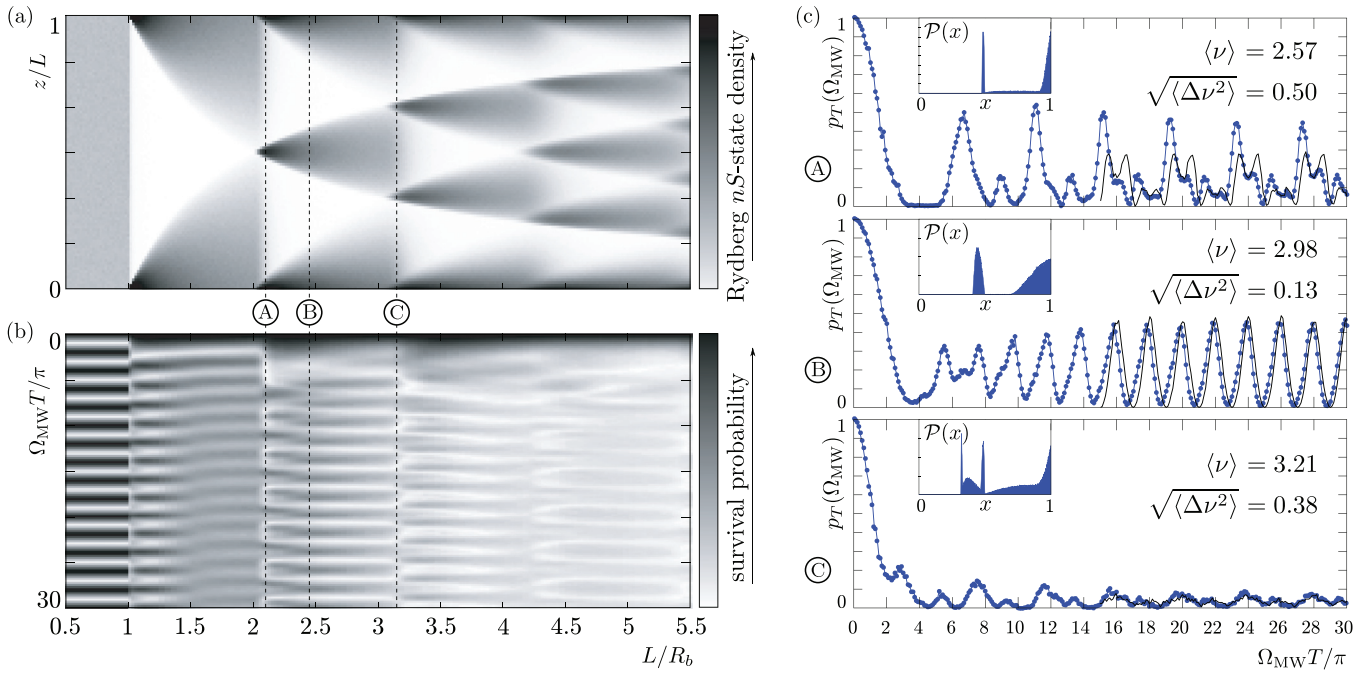

FIG. 2. (Color online) (a) Numerically calculated density distribution of Rydberg atoms after laser excitation as a function of the system length L measured in units of the blockade radius R_b. (b) Survival probability $p_T(\Omega_{\rm MW})$ as a function of L/R_b and microwave Rabi frequency $\Omega_{\rm MW}$. The colormaps in panels (a) and (b) range from 0 (white) to 1 (black). (c) Cuts through the density plot shown in (b) for three different system sizes indicated by the encircled capital letters. The corresponding mean $\langle\nu\rangle$ and variance $\sqrt{\langle\Delta\nu^2\rangle}$ of the Rydberg atom number distribution are indicated in the panels. The blue symbols show numerical results from the Hamiltonian given in Eq. (2) and the solid black lines are obtained using the effective Hamiltonian (5) valid for large $\Omega_{\rm MW}$. The statistical distribution of the dipole-dipole interaction energy between atom pairs is shown in the insets. For better visibility we show the distributions as a function of $x = (\mathcal{V}R_b^3/\mu^2)^{1/3}$, i.e., the third root of the interaction strength at the blockade distance R_b. The data shown in panels (b) and (c) were obtained by averaging over 400 initial configurations generated by Monte Carlo sampling. In (b) and (c) the dipole-dipole interaction strength, $V(R_b)$, for an atom pair separated by R_b is $V(R_b)T = 15$.

reveals interesting insights into the physics of the driven exciton system. Following [28], we numerically determine $p_T(\Omega_{\rm MW})$ for varying strength of the microwave coupling and in addition as a function of the system length for fixed time T and blockade radius R_b. The results are summarized in Fig. 2(b), where the dipole-dipole interaction strength is chosen such that for two atoms separated by the blockade radius $V(R_b)T = 15$. Additionally, we present cuts through these data for three selected values of the system length in Fig. 2(c). The survival probability exhibits a rich structure as L and $\Omega_{\rm MW}$ are varied, which, in particular, is clearly correlated to the distribution of Rydberg atoms shown in Fig. 2(a). This is most apparent when the system length is close to an integer multiple of the blockade radius, i.e., when an additional Rydberg atom can "fit" into the system. Here, the change in the Rydberg density distribution becomes strikingly visible through a phase jump in the survival probability pattern.

Beyond this global feature, each cut of $p_T(\Omega_{\rm MW})$, taken at a fixed system length L, exhibits three distinct regimes as a function of the microwave Rabi frequency [cf. panels of Fig. 2(c)]. For very small $\Omega_{\rm MW}$ the dynamics is dominated by excitonic energy transfer induced by the dipole-dipole interaction. The system can then be regarded as a number of exciton bands that are weakly coupled by the microwave field. Here, $p_T(\Omega_{\rm MW})$ decreases monotonically with increasing $\Omega_{\rm MW}$. When the microwave Rabi frequency becomes comparable to the mean dipole-dipole energy $\langle\mathcal{V}\rangle$, the survival probability exhibits a rather intricate pattern. Here, as well as in the previous regime, the exact details of $p_T(\Omega_{\rm MW})$ are very sensitive to the particular distribution of the Rydberg atoms [cf. Figs. 2(a) and 2(b)]. This sensitivity is caused by the distance dependence of the dipole-dipole interaction, which essentially probes the pair distribution function $\mathcal{R}^{(2)}(z,z')$ of the Rydberg gas. To see this one can use the formal expression (1) for $|\Psi_0\rangle$ to express the survival probability. The resulting expression depends on the distributions $\rho^{(\nu)}(z_1,\ldots,z_\nu) = |g^{(\nu)}(z_1,\ldots,z_\nu)|^2$ in each particle number subspace, which together determine the pair distribution function through

$$\mathcal{R}^{(2)}(z,z') = \sum_{\nu=2}^{\nu_{\rm max}} \int dz_3 \cdots dz_\nu \rho^{(\nu)}(z,z',z_3,\ldots,z_\nu). \qquad (3)$$

Since the interaction potential has a strong nonlinear dependence on the interparticle distance, even small differences in $\mathcal{R}^{(2)}(z,z')$ lead to a significantly modified statistical distribution

$$\mathcal{P}(\mathcal{V}) = \int dz dz' \delta(\mathcal{V} - \mu^2/|z-z'|^3)\mathcal{R}^{(2)}(z,z') \qquad (4)$$

of the dipole-dipole interaction energy $\mathcal{V}$ as shown in the insets of the panels in Fig. 2(c).

Finally, for $\Omega_{\rm MW} \gg \langle\mathcal{V}\rangle$ the survival probability shows regular oscillations. Most interestingly, as a general trend the

amplitude of these oscillations decreases with increasing number of Rydberg atoms in the gas [cf. rightmost part of Fig. 2(b)]. This effect seems counterintuitive as for $\Omega_{\rm MW}/\langle\mathcal{V}\rangle \gg 1$ one might expect to enter a noninteracting regime in which the microwave drives coherent oscillations between the single atom states $|nS\rangle$ and $|n'P\rangle$. This would always lead to oscillation of $p_T(\Omega_{\rm MW})$ with full contrast. However, this is a misconception as even for $\Omega_{\rm MW}/\langle\mathcal{V}\rangle \gg 1$ interactions still play a significant role. This can be understood by deriving the effective Hamiltonian in the limit $V_{ij} \ll \Omega_{\rm MW}$, starting from Eq. (2). To this end, we rotate the spin basis via a unitary transformation $U = \bigotimes_j U_j$ with $U_j = \exp(i\pi\sigma_j^y/4)$, which diagonalizes the single-body part of H. In the transformed Hamiltonian $UHU^\dagger$ we neglect nonresonant terms of the form $\sigma_i^+\sigma_j^+$ and $\sigma_i^-\sigma_j^-$ that correspond to the simultaneous (de)excitation of a spin pair. Within this approximation we find that the effective Hamiltonian is that of the spin-1/2 XXZ model,

$$H_{\rm eff} = \frac{\Omega_{\rm MW}}{2}\sum_i \sigma_i^z + \sum_{ij,(i\neq j)} \frac{V_{ij}}{4}\left(\sigma_i^x\sigma_j^x + \sigma_i^y\sigma_j^y + 2\sigma_i^z\sigma_j^z\right). \tag{5}$$

This Hamiltonian consists of two commuting parts and thus the microwave driving and the residual dipole-dipole interaction can be treated independently. This shows that no matter how strong $\Omega_{\rm MW}$ there will always be a nontrivial excitonic dynamics. To illustrate this further let us assume that we are in a regime where the number of Rydberg atoms $\nu_{\rm Ryd}$ is integer and hence not fluctuating, as, e.g., is shown in the middle panel of Fig. 2(c). The survival amplitude can now be expressed in terms of a Fourier series, $\langle\Psi_0|e^{-iH_{\rm eff}T}|\Psi_0\rangle = B(T) + 2\sum_{m=0}^{M} A_m(T)\cos(\epsilon_m T)$, with $\epsilon_m = \Omega_{\rm MW}(m - \nu_{\rm Ryd}/2)$ and coefficients $A_m(T)$ and $B(T)$, which exclusively depend on the phases $V_{ij}T$ but not on $\Omega_{\rm MW}$. If $\nu_{\rm Ryd}$ is odd the summation runs to $M = (\nu_{\rm Ryd} - 1)/2$ otherwise to $M = \nu_{\rm Ryd}/2 - 1$. In the case of odd $\nu_{\rm Ryd}$ the symmetry of the Hamiltonian (5) with respect to a global spin-flip operation imposes $B(T) = 0$. Hence, in this case the survival probability is exactly zero when $\Omega_{\rm MW}T/\pi$ is an odd integer, which is clearly visible in the middle panel of Fig. 2(c). Note, that in general only if $V_{ij} = 0$ the Fourier series can be summed analytically and one consequently obtains the familiar expression for Rabi oscillations of noninteracting particles $|\langle\Psi_0|e^{-iH_{\rm eff}T}|\Psi_0\rangle|^2 = \cos^{2\nu_{\rm Ryd}}(\Omega_{\rm MW}T)$.

IV. EXPERIMENT

We will now conclude with a qualitative comparison of our theoretical results with experimental data. Full details of the experiment can be found in [28]. In brief, laser-cooled ^{87}Rb atoms are loaded into an optical dipole trap forming an elongated cloud with $w_z \approx 20\,\mu$m and $w_r \approx 0.8\ \mu$m, where w is the standard deviation of the density distribution. Rydberg $60S_{1/2}$ states are excited with a two-photon transition via the intermediate $5P_{3/2}$ state (see Fig. 3). For the experimental parameters the blockade radius is $R_b \approx 7\,\mu$m $\gg w_r$ and hence the setup is quasi-one-dimensional as illustrated in Fig. 1(b). The optical excitation fields are applied for a sufficiently long time that saturation is reached (see right inset of Fig. 3 and corresponding caption). This corresponds to step 1, i.e., the preparation of the emergent lattice. Subsequently, the lasers are switched off and a microwave field (step 2, driving the exciton dynamics), couples the states $|60S_{1/2}\rangle$ and $|59P_{3/2}\rangle$, for a time $T = 150$ ns. After step 2 the Rydberg excitations in state $60S_{1/2}$ are converted into photons by switching on the control field, see [28]. The resulting photon-retrieval probability P is proportional to the survival probability $p_T(\Omega_{\rm MW})$ [28] and plotted in Fig. 3 as a function of the microwave Rabi frequency, $\Omega_{\rm MW}$.

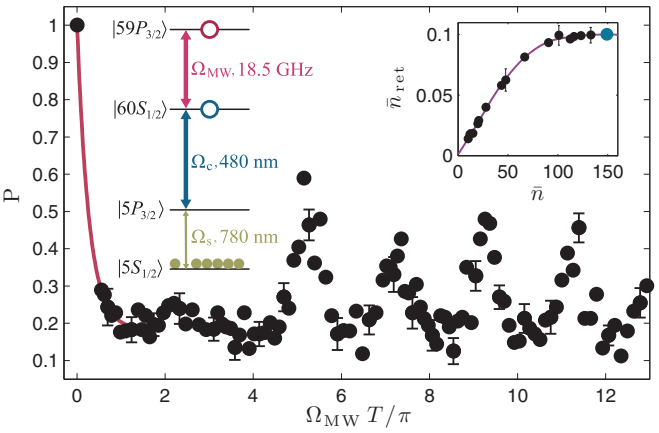

FIG. 3. (Color online) Experimentally measured photon retrieval probability P as a function of the microwave Rabi frequency $\Omega_{\rm MW}$. The duration of the microwave pulse, $T = 150$ ns, is fixed. Inset: (Left) Excitation scheme used in the experiment. The Rydberg $60S_{1/2}$ state is reached by a two-photon transition via the $5P_{3/2}$ state. A microwave field couples the $60S_{1/2}$ state to the $59P_{3/2}$ state. (Right) As the number of photons $\bar{n}$ in the signal field (proportional to the Rabi frequency Ω_s and pulse duration) is increased, the number of retrieved photons $\bar{n}_{\rm ret}$ saturates in the absence of microwave driving. The data shown in the main plot are obtained well within this saturated regime (blue point). The lines are a guide to the eye.

Remarkably, these data show qualitatively the same features as the discussed theoretical model, i.e., a quick decay of the survival probability, followed by increasingly regular oscillations. In fact, the shape of the curve follows quite closely the behavior depicted in the middle panel of Fig. 2(c). This is despite the fact that details of the experiment, e.g., the excitation scheme and the Gaussian atomic density distribution, differ from the underlying theoretical model.

V. CONCLUSION

In this work we have studied the dynamics of a two-step protocol that consists (i) of photoexciting Rydberg atoms from an one-dimensional ultracold gas and (ii) subsequently inducing excitonic energy transfer in the highly correlated Rydberg gas using a microwave field. In the regime of weak microwave driving we have shown that the exciton dynamics strongly depends on the spatial arrangement of the Rydberg atoms. This connection opens up the possibility of using the second step of our protocol as a diagnostic tool for mapping out the spatial structure of highly correlated Rydberg gases. In the opposite limit of strong microwave driving we have shown that the dynamics of the system is governed by the Hamiltonian of the XXZ model. This highlights the applicability of simple models to describe and understand complex experiments to investigate nonequilibrium exciton dynamics in ultracold Rydberg systems.

ACKNOWLEDGMENTS

We thank B. Olmos for useful comments on the manuscript. S.B. and T.F. acknowledge funding from EPSRC. D.M. and C.S.A. acknowledge support from EPSRC, Durham University and the EU Marie Curie ITN COHERENCE. I.L. acknowledges funding by EPSRC, the Leverhulme Trust, and the EU-FET Grant QuILMI 295293. C.A. acknowledges support through the Alexander von Humboldt Foundation.

APPENDIX: CONFIGURATION-SELECTION ALGORITHM

The Monte Carlo algorithm that we have used to obtain our numerical data relies on the generation of excitation configurations (that are compatible with the Rydberg blockade) "on the fly." It is composed of a preparation stage and an actual drawing stage.

1. Preparation stage

In the first stage we prepare two tables [$c(j,k)$ and $n(j)$] that we will use to quickly generate random configurations in the second stage of our algorithm. To this end we label the N atoms from left to right with an index j and define $c(j,k)$ to be the number of allowed configurations (compatible with the blockade) with $k \geqslant 0$ excitations in the index range $[j,N]$ and zero excitations in the range $[1,j-1]$. Furthermore, we define $n(j) > j$ as the index of the first atom to the right of a Rydberg atom at position j that lies outside the blockade radius. With these definitions the following recursive relation holds for $k > 1$:

$$c(j,k) = \sum_{q=j}^{N} c(n(q),k-1), \tag{A1}$$

with initial conditions $c(j,0) = 1$ and $c(j,1) = N - j + 1$. This permits the calculation of the total number $\mathcal{N}$ of allowed configurations as well as the fraction p_k of configurations with exactly k excitations, according to the formulas $\mathcal{N} = \sum_{k\geqslant 0} c(1,k)$ and $p_k = c(1,k)/\mathcal{N}$.

To illustrate the procedure, let us take $N = 7$ atoms spaced as in the following diagram (where the distance between two vertical bars is one blockade radius):

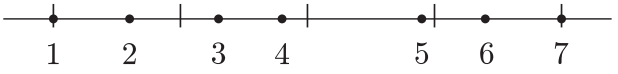

The corresponding values of $n(j)$ and $c(j,k)$ are then

j	$n(j)$
1	3
2	4
3	5
4	5
5	7
6	
7	

$j\backslash k$	0	1	2	3	4
1	1	7	16	13	3
2	1	6	11	6	1
3	1	5	7	2	
4	1	4	4	1	
5	1	3	1		
6	1	2			
7	1	1			
p_k	$\frac{1}{40}$	$\frac{7}{40}$	$\frac{16}{40}$	$\frac{13}{40}$	$\frac{3}{40}$

Therefore, $\nu_{\max} = 4$, $\mathcal{N} = \sum_k c(1,k) = 40$.

Note that the $\mathcal{N}$ actual configurations are never explicitly generated (as the resources in time and memory would scale exponentially with N), but for the sake of clarity the 40 possible ones are

# excit	# config	actual configurations (excited atoms shown in parentheses)
0	1	();
1	7	(1), (2), (3), (4), (5), (6), (7);
2	16	(13), (14), (15), (16), (17), (24), (25), (26), (27), (35), (36), (37), (45), (46), (47), (57);
3	13	(135),(136),(137),(145),(146),(147),(157), (245),(246),(247),(257),(357),(457);
4	3	(1357), (1457), (2457).

2. Drawing stage

Once the $c(j,k)$ table is ready, we can use it to randomly sample the space of allowed configurations. To this end we draw a random integer m in the range $[1,\mathcal{N}]$. To uniquely ascribe a specific configuration to m we use the convention that configurations are first ordered according to the number ν of excitations and then lexicographically over the indexes of excited atoms. The search is implemented first scanning the entries $c(1,k)$ till ν is determined, then using the entries $c(j,\nu)$ to find the actual excitation positions. In C pseudocode the algorithm reads

```
k=0; j=1;
while (m>c(1,k)) {m-=c(1,k); ++k;} // step 1
while (k>1) {q=j; // step  2
  while (m>c(n(q),k-1)) {m-=c(n(q),k-1); ++q;}
  mark_as_excited(q); j=n(q); --k;}
if (k>0) mark_as_excited(j+m-1);
```

Let us see how this works in the example for $m = 35$:

[$m = 35$] $m > c(1,0) = 1 \Rightarrow$ not the configuration with zero excitations, then update $m \to m - c(1,0) = 34$;

[$m = 34$] $m > c(1,1) = 7 \Rightarrow$ not a configuration with one excitation, then update $m \to m - c(1,1) = 27$;

[$m = 27$] $m > c(1,2) = 16 \Rightarrow$ not a configuration with two excitations, then update $m \to m - c(1,2) = 11$;

[$m = 11$] $m \leqslant c(1,3) = 13 \Rightarrow$ the selected configuration has $\nu = 3$ excitations; let us look for their indexes;

[$m = 11$] $m > c(n(1),\nu - 1) = 7 \Rightarrow$ the first index is larger than 1, then update $m \to m - c(n(1),\nu - 1) = 4$;

[$m = 4$] $m \leqslant c(n(2),\nu - 1) = 4 \Rightarrow$ the first index is $j_1 = 2$; let us look for the second one [from $n(j_1) = 4$ on];

[$m = 4$] $m > c(n(4),\nu - 2) = 3 \Rightarrow$ the second index is larger than 4, then update $m \to m - c(n(4),\nu - 2) = 1$;

[$m = 1$] $m \leqslant c(n(5),\nu - 2) = 1 \Rightarrow$ the second index is $j_2 = 5$; let us look for the last one;

[$m = 1$] the last index is just $n(j_2) + m - 1 = 7 + 1 - 1 = 7$, then the selected configuration is (257).

Using this procedure repeatedly, we can generate a random sequence $\mathcal{S} = \{m_1, m_2, \ldots, m_K\}$ of K allowed configurations, where each configuration is drawn with equal probability $1/\mathcal{N}$. Classical observables like the local Rydberg density $\langle n_i \rangle$ or density-density correlations $\langle n_i n_j \rangle$ can then be determined as

$$\langle n_i \rangle \approx \frac{1}{K} \sum_{\mathcal{S}} (n_i)_{\mathcal{S}}\,, \tag{A2}$$

$$\langle n_i n_j \rangle \approx \frac{1}{K} \sum_{\mathcal{S}} (n_i n_j)_{\mathcal{S}}. \tag{A3}$$

[1] M. C. Cross and P. C. Hohenberg, Rev. Mod. Phys. **65**, 851 (1993).
[2] G. D. Scholes, Annu. Rev. Phys. Chem. **54**, 57 (2003).
[3] G. S. Engel, T. R. Calhoun, E. L. Read, T.-K. Ahn, T. Mancal, Y.-C. Cheng, R. E. Blankenship, and G. R. Fleming, Nature (London) **446**, 782 (2007).
[4] G. D. Scholes and G. Rumbles, Nat. Mater. **5**, 683 (2006).
[5] R. Mottl, F. Brennecke, K. Baumann, R. Landig, T. Donner, and T. Esslinger, Science **336**, 1570 (2012).
[6] M. Gring, M. Kuhnert, T. Langen, T. Kitagawa, B. Rauer, M. Schreitl, I. Mazets, D. A. Smith, E. Demler, and J. Schmiedmayer, Science **337**, 1318 (2012).
[7] S. Trotzky, Y.-A. Chen, A. Flesch, I. P. McCulloch, U. Schollwock, J. Eisert, and I. Bloch, Nat. Phys. **8**, 325 (2012).
[8] M. D. Lukin, M. Fleischhauer, R. Côté, L. M. Duan, D. Jaksch, J. I. Cirac, and P. Zoller, Phys. Rev. Lett. **87**, 037901 (2001).
[9] M. Saffman, T. G. Walker, and K. Mølmer, Rev. Mod. Phys. **82**, 2313 (2010).
[10] J. D. Pritchard, D. Maxwell, A. Gauguet, K. J. Weatherill, M. P. A. Jones, and C. S. Adams, Phys. Rev. Lett. **105**, 193603 (2010).
[11] S. Sevincli, N. Henkel, C. Ates, and T. Pohl, Phys. Rev. Lett. **107**, 153001 (2011).
[12] D. Petrosyan, J. Otterbach, and M. Fleischhauer, Phys. Rev. Lett. **107**, 213601 (2011).
[13] Y. O. Dudin and A. Kuzmich, Science **336**, 887 (2012).
[14] T. Peyronel, O. Firstenberg, Q.-Y. Liang, S. Hofferberth, A. V. Gorshkov, T. Pohl, M. D. Lukin, and V. Vuletic, Nature (London) **488**, 57 (2012).
[15] A. V. Gorshkov, R. Nath, and T. Pohl, Phys. Rev. Lett. **110**, 153601 (2013).
[16] C. Ates and I. Lesanovsky, Phys. Rev. A **86**, 013408 (2012).
[17] D. Breyel, T. L. Schmidt, and A. Komnik, Phys. Rev. A **86**, 023405 (2012).
[18] M. Gärttner, K. P. Heeg, T. Gasenzer, and J. Evers, Phys. Rev. A **86**, 033422 (2012).
[19] M. Höning, D. Muth, D. Petrosyan, and M. Fleischhauer, Phys. Rev. A **87**, 023401 (2013).
[20] A. Schwarzkopf, R. E. Sapiro, and G. Raithel, Phys. Rev. Lett. **107**, 103001 (2011).
[21] Y. O. Dudin, F. Bariani, and A. Kuzmich, Phys. Rev. Lett. **109**, 133602 (2012).
[22] P. Schauß, M. Cheneau, M. Endres, T. Fukuhara, S. Hild, A. Omran, T. Pohl, C. Gross, S. Kuhr, and I. Bloch, Nature (London) **491**, 87 (2012).
[23] I. Mourachko, D. Comparat, F. de Tomasi, A. Fioretti, P. Nosbaum, V. M. Akulin, and P. Pillet, Phys. Rev. Lett. **80**, 253 (1998).
[24] W. R. Anderson, J. R. Veale, and T. F. Gallagher, Phys. Rev. Lett. **80**, 249 (1998).
[25] W. Li, P. J. Tanner, and T. F. Gallagher, Phys. Rev. Lett. **94**, 173001 (2005).
[26] C. S. E. van Ditzhuijzen, A. F. Koenderink, J. V. Hernández, F. Robicheaux, L. D. Noordam, and H. B. van Linden van den Heuvell, Phys. Rev. Lett. **100**, 243201 (2008).
[27] J. Nipper, J. B. Balewski, A. T. Krupp, B. Butscher, R. Löw, and T. Pfau, Phys. Rev. Lett. **108**, 113001 (2012).
[28] D. Maxwell, D. J. Szwer, D. Paredes-Barato, H. Busche, J. D. Pritchard, A. Gauguet, K. J. Weatherill, M. P. A. Jones, and C. S. Adams, Phys. Rev. Lett. **110**, 103001 (2013).
[29] J. S. Frasier, V. Celli, and T. Blum, Phys. Rev. A **59**, 4358 (1999).
[30] F. Robicheaux, J. V. Hernández, T. Topçu, and L. D. Noordam, Phys. Rev. A **70**, 042703 (2004).
[31] O. Mülken, A. Blumen, T. Amthor, C. Giese, M. Reetz-Lamour, and M. Weidemüller, Phys. Rev. Lett. **99**, 090601 (2007).
[32] M. Müller, L. Liang, I. Lesanovsky, and P. Zoller, New J. Phys. **10**, 093009 (2008).
[33] S. Wüster, C. Ates, A. Eisfeld, and J. M. Rost, Phys. Rev. Lett. **105**, 053004 (2010).
[34] S. Wüster, C. Ates, A. Eisfeld, and J. M. Rost, New J. Phys. **13**, 073044 (2011).
[35] T. Scholak, T. Wellens, and A. Buchleitner, J. Phys. B **44**, 184012 (2011).
[36] M. Kiffner, H. Park, W. Li, and T. F. Gallagher, Phys. Rev. A **86**, 031401 (2012).
[37] F. Bariani, Y. O. Dudin, T. A. B. Kennedy, and A. Kuzmich, Phys. Rev. Lett. **108**, 030501 (2012).
[38] D. Petrosyan, M. Höning, and M. Fleischhauer, Phys. Rev. A **87**, 053414 (2013).
[39] I. Lesanovsky, B. Olmos, and J. P. Garrahan, Phys. Rev. Lett. **105**, 100603 (2010).
[40] C. Ates, J. P. Garrahan, and I. Lesanovsky, Phys. Rev. Lett. **108**, 110603 (2012).
[41] S. Ji, C. Ates, J. P. Garrahan, and I. Lesanovsky, J. Stat. Mech.: Theory Expt. (2013) P02005.